

Improved CCD Standard Fields

S. C. ODEWAHN, C. BRYJA, AND R. M. HUMPHREYS

Department of Astronomy, University of Minnesota, 116 Church Street S. E., Minneapolis, Minnesota 55455

Electronic mail: sco@aps1.spa.umn.edu, clai@aps1.spa.umn.edu, roberta@aps1.spa.umn.edu

Received 1991 November 15; accepted 1992 April 9

ABSTRACT. We have combined multiple nights of charge-coupled device (CCD) observations of NGC 7790, NGC 7006, and NGC 4147 in order to establish a deep sequence of photometric standards whose errors have been objectively derived through statistical comparisons. In addition to extending these previously studied fields to a fainter limit, we have increased the range in observed color, making the new mean sequences more suitable for deriving photometric transformation coefficients.

1. INTRODUCTION

Accurate photometry of compact stellar fields is extremely useful for the purpose of calibrating all-sky charge-coupled device (CCD) observations. Because of the time involved in obtaining CCD image frames, as opposed to integrations with a single channel photometer, it is more efficient to obtain multiple standard star observations in a single field. For the purpose of deriving photometric transformation coefficients with these observations the standard fields must have photometric errors which are small and objectively determined, and the range in stellar color must be adequately large to allow for the accurate fit of color transformation equations. Such was the intent of Christian et al. (1985, hereafter referred to as C85), when they published photometric photometry of compact fields in the

area of several galactic and globular clusters. As noted by these authors, the problem of accounting for field crowding effects is difficult with a classical single channel photometer, and the time involved in obtaining photometry for a large number of stars with such a device is prohibitive. Hence, many of the C85 fields are composed of a relatively small number of stars in a rather restricted color range.

We have used a number of the C85 fields in the first phase of a large program of all-sky CCD photometry designed to establish photometric sequences near the centers of Palomar Sky Survey fields. These sequences will be used in the calibration of the automated plate scanner (APS) measurements of the Palomar Sky Survey (Humphreys et al. 1991) for the purpose of compiling both stellar and

TABLE 1
Summary of Observations

field	d/m/y	σ_V	σ_{B-V}	σ_{V-R}	field	d/m/y	σ_V	σ_{B-V}	σ_{V-R}
N4147	08/01/89	0.142	0.112	0.098	N7790	08/09/89	0.028	0.024	0.019
N4147	02/04/89	0.091	0.122	0.092	N7790	23/09/89	0.026	0.011	0.017
N4147	03/04/89	0.077	0.058	0.030	N7790	27/10/89	0.038	0.025	0.027
N4147	13/04/89	0.061	0.074	0.063	N7790	28/10/89	0.029	0.007	0.024
N4147	25/04/89	0.051	0.050	0.041	N7790	29/10/89	0.042	0.030	0.042
N4147	27/04/89	0.066	0.090	0.050	N7790	30/10/89	0.036	0.034	0.028
N4147	28/04/89	0.057	0.059	0.066	N7790	01/11/89	0.030	0.018	0.047
N4147	30/04/89	0.061	0.063	0.046	N7790	22/11/89	0.032	0.027	0.020
N4147	04/12/88	0.076	0.067	0.048	N7790	25/11/89	0.033	0.013	0.020
					N7790	26/11/89	0.031	0.020	0.011
					N7790	27/11/89	0.043	0.036	0.024
N7006	27/09/89	0.024	0.042	0.042	N7790	28/11/89	0.030	0.016	0.016
N7006	28/09/89	0.020	0.037	0.025	N7790	03/12/89	0.055	0.048	0.042
N7006	29/09/89	0.026	0.047	0.025	N7790	05/12/89	0.054	0.034	0.059
N7006	30/09/89	0.018	0.033	0.018	N7790	19/12/89	0.050	0.032	0.034
N7006	09/10/89	0.020	0.025	0.025	N7790	20/12/89	0.035	0.014	0.017
N7006	10/10/89	0.071	0.048	0.044	N7790	31/12/89	0.036	0.033	0.032
N7006	24/10/89	0.014	0.051	0.013	N7790	01/01/90	0.039	0.021	0.025
N7006	26/10/89	0.055	0.053	0.038	N7790	24/01/90	0.034	0.051	0.033
N7006	22/11/89	0.032	0.027	0.020	N7790	25/01/90	0.040	0.035	0.036
N7006	25/11/89	0.033	0.013	0.020	N7790	27/01/90	0.059	0.052	0.024

galaxy catalogs of the northern sky (Pennington et al. 1991). We have obtained a large number of multiple sets of *BVR* CCD images for three of the fields in C85. The two-dimensional images allow us to detect and exclude stars which are plagued by crowding problems, and multiple observations allow us to compare photometry from many different nights and hence objectively establish the internal errors of the photometry. Because our observations are tied to the zero point of the C85 photometry, we cannot hope to detect or correct for any systematic zero-point errors, but by combining many nights into a mean photometric set, we will greatly reduce the accidental errors present in the C85 data. In addition, we can establish a large number of fainter standards in these fields, providing more stars covering a wider color range for photometric solutions.

In the following sections we describe the methods used to observe and reduce the photometry for three of the C85 standard fields: NGC 7790, NGC 7006, and NGC 4147. We present a statistical analysis of these data designed to detect discrepant observations due to crowding effects or variability, and to determine the observational scatter in the photometry as a function of magnitude. Finally, we present tables of mean photometry for these fields.

2. OBSERVATIONS AND REDUCTION

All of the CCD observations used to produce the mean photometry sets discussed here were obtained with a 320 × 512 RCA SID501EX CCD attached to the Cassegrain focus of the 0.6-m reflector at the University of New Mexico's Capilla Peak Observatory. A filter set designed to duplicate very closely the Cousins *BVR* bandpasses (Beckert and Newberry 1989) was used during each night of observations. This filter set and CCD combination resulted in rather small coefficients when transforming the instrumental magnitudes to the standard Cousins system. Table 1 gives the date of observation, the standard field observed, and the root-mean-square (rms) scatter in the photometric transformation solutions. Each set of observations consists of two *B*, two *V*, and two *R* CCD images. For the NGC 4147 and NGC 7006 images, *B*, *V*, and *R* band integration times were 900, 600, and 300 s, respectively. For the brighter stars of NGC 7790, we used integration times of 300, 150, and 60 s, respectively. Extinction star observations of at least two Landolt (1973) standards per night were made at 2–3 airmass values covering the range $1.10 < X < 2.0$. Due to the brightness of these standards (typically $V=10-12$), integration times ran from 10 to 90 s. In order to avoid charge trapping effects associated with the RCA chip in short exposures, all images were preflashed to an approximate level of 780 electrons at the start of each integration. Pairs of images were obtained in each bandpass in order to detect errors associated with cosmic-ray defects, as well as to allow an assessment of the internal instrumental photometric errors for each observed field. It must be noted that the NGC 4147 observations were obtained prior to the adoption of the CCD preflashing technique. The length of these integrations was sufficient to avoid charge trapping problems, but short extinction star

integrations were impossible and hence we have adopted mean atmospheric extinction coefficients for these nights.

A total of 21 nights of observations has been collected for NGC 7790, 10 nights for NGC 7006, and 9 nights for NGC 4147. The photometry of C85 was used to calibrate the NGC 7790 and NGC 4147 images. Revised CCD photometry of NGC 7006, kindly provided prior to publication by L. Davis (1990, private communication), was used to calibrate the photometry for that field. Instrumental magnitudes were converted to the standard Cousins system via the following transformation equations:

$$V = v - k_v X + C_v(B - V) + z_v, \quad (1)$$

$$B - V = C_{bv}[(b - v)(1 - k'_{bv} X) - k_{bv} X] + z_{bv}, \quad (2)$$

$$V - R = C_{vr}[(v - r) - k_{vr} X] + z_{vr}. \quad (3)$$

Lower case letters indicate instrumental magnitudes. For each night, the color extinction term was assumed to be $k'_{bv} = -0.025$, but values of the first-order extinction terms (k_v, k_{bv}, k_{vr}) were determined through multiple airmass observations of Landolt standards. It should be noted that on two nights, both NGC 7006 and NGC 7790 were observed, and the resulting photometric zero points (holding the extinction and color transformation terms fixed) derived independently for each field were in good agreement within the derived statistical errors. Transformation and extinction coefficients determined independently for each night were generally found to be in excellent agreement. In a few cases, the derived extinction coefficients were found to be poorly determined, and here we adopted mean coefficients computed with extinction solutions from ten excellent nights.

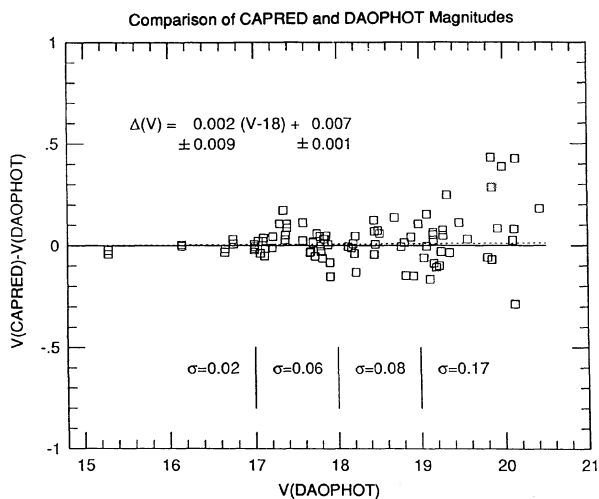


FIG. 1—A comparison between instrumental magnitudes determined with DAOPHOT and with the aperture integration technique used in this work. Magnitude residuals, $m(\text{DAOPHOT}) - m(\text{CAPRED})$, are plotted as a function of $m(\text{DAOPHOT})$. No strong trends are evident to the faintest magnitude values at $V=20$. The solid line represents a mean residual of zero, the dashed line represents a least-squares regression line fitted to the residuals.

Reduction of the CCD images was performed in an automated fashion using a code known as CAPRED developed for the APS CCD photometry project. Initial processing followed standard procedure and included subtraction of a high signal-to-noise bias frame to remove a constant fixed bias pattern and flat field correction using master flat field frames produced from multiple dawn and/or dusk sky flats. Stellar images were detected automatically using a background thresholding algorithm. Only images having a peak brightness of $\beta\sigma_s$ above the local background and having at least a minimum number of connected pixel columns (N_{pix}), were selected for measurement. Throughout this work, we have adopted values of $\beta=3.0$ and $N_{\text{pix}}=4$. The local sky noise σ_s is taken to be the standard deviation of background pixel counts, which is established through an iterative rejection about the mode.

Instrumental magnitudes are derived through integration in simulated apertures. The aperture radius varies with the stellar brightness and is set to match the radius at which the mean sky subtracted pixel values fall to a level of 50% of the local sky noise. In this case, the sky noise level is taken to be the standard deviation of pixels values measured in a sky annulus centered on each star. This technique is required in the case of faint stellar images where the integrated stellar flux can be easily overwhelmed in the

sky subtraction stage due to small errors in the sky determination. The use of a variable aperture requires that an aperture correction be applied in order that all instrumental magnitudes be in the same system. In our case, a single gaussian fit is applied to all bright stars in each image in order to model the outer wings of the stellar profile. Based on the width, σ_r , of this mean profile, we may calculate the integrated flux contained in an image beyond a given radius. Such a correction is negligible for bright stars ($V \leq 18.0$), where the aperture generally extends to the $3\sigma_r$ radius, but this correction becomes significant at fainter levels where the estimated optimum aperture size may be only $2\sigma_r$. It should be noted that a minimum aperture radius of 3 pixels (corresponding to $2''$) has been imposed in the code in order that very faint stars not be measured with unreasonably small aperture.

We were motivated to adopt this rather simple aperture integration scheme because of its relative ease in implementation. Because of the large number of CCD fields which must be processed in the POSS calibration field project, a completely automated reduction package was deemed necessary. The use of a two-dimensional point spread function fitting program such as DAOPHOT or DAOGROW (Stetson

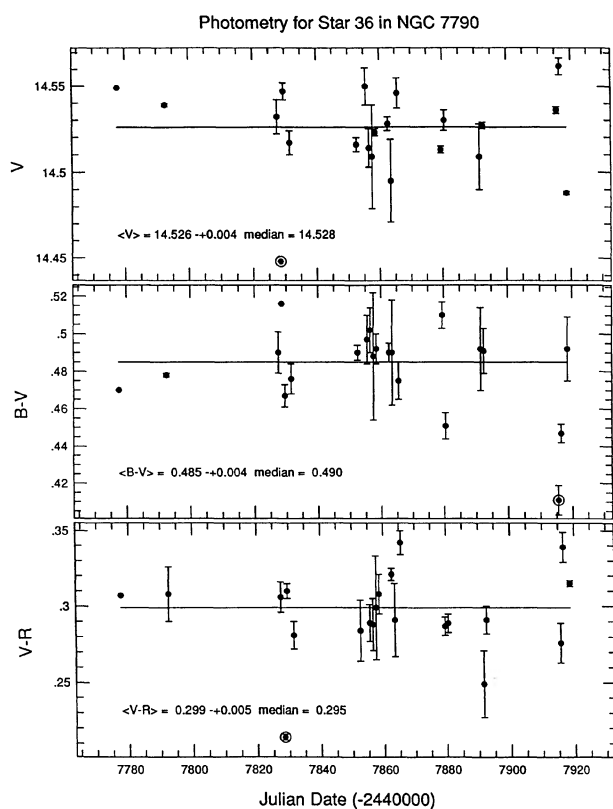


FIG. 2—Magnitude vs Julian Date for a typical set of magnitude and color measurements in the NGC 7790 photometry sample. Circled points indicate data eliminated in the rejection process. Plots such as this were used to confirm that the rejected points were indeed discrepant observations.

TABLE 2
Mean Photometry for NGC 4147

name	V	m.e.	n	B - V	m.e.	n	V - R	m.e.	n
6	16.730	0.013	8	0.773	0.010	8	0.496	0.011	9
9	18.308	0.025	9	0.625	0.031	8	0.429	0.030	9
11	16.785	0.009	8	0.779	0.017	8	0.472	0.013	9
12	17.722	0.013	8	1.107	0.019	9	0.748	0.010	8
14	17.358	0.007	8	0.054	0.007	8	-0.066	0.015	9
15	16.734	0.005	8	0.132	0.013	9	0.017	0.010	8
102	18.997	0.052	8	0.583	0.103	8	0.366	0.049	8
103	19.038	0.026	7	0.571	0.075	7	0.560	0.053	7
104	18.558	0.022	6	1.296	0.027	6	0.884	0.039	6
106	19.191	0.061	8	0.529	0.083	8	0.392	0.074	8
107	18.895	0.020	8	0.600	0.077	8	0.409	0.034	8
109	17.575	0.013	8	0.733	0.017	8	0.402	0.026	8
110	18.823	0.027	8	0.629	0.071	8	0.488	0.063	9
111	20.138	0.061	8	0.346	0.055	8	0.105	0.070	8
112	19.842	0.064	9	0.377	0.081	8	0.224	0.088	9
114	18.967	0.013	8	0.680	0.036	9	0.330	0.045	9
115	18.283	0.012	8	0.664	0.019	8	0.415	0.014	9
119	17.457	0.007	9	0.687	0.017	9	0.493	0.014	9
120	15.034	0.009	8	1.034	0.018	8	0.618	0.015	9
121	17.996	0.015	8	1.436	0.015	8	0.942	0.024	9
122	16.381	0.008	8	0.632	0.013	9	0.431	0.013	8
123	19.637	0.032	9	0.679	0.069	8	0.262	0.066	8
124	16.984	0.007	6	0.479	0.014	6	0.320	0.007	6
125	18.857	0.039	8	0.672	0.029	7	0.382	0.065	7
126	18.017	0.032	8	0.711	0.035	8	0.444	0.033	8
127	17.903	0.013	9	0.655	0.010	8	0.402	0.019	8
128	18.589	0.027	9	0.649	0.067	8	0.521	0.041	8
129	17.528	0.031	9	0.748	0.020	8	0.427	0.024	8
130	17.192	0.013	8	0.014	0.015	8	-0.059	0.015	8
131	18.310	0.023	8	0.663	0.024	8	0.447	0.029	9
132	17.572	0.015	8	0.671	0.016	9	0.464	0.016	8
133	17.466	0.012	8	0.653	0.012	8	0.443	0.015	9
134	17.038	0.070	9	0.247	0.028	8	0.164	0.037	9
135	17.287	0.051	8	-0.093	0.032	8	-0.062	0.052	8
136	16.894	0.016	7	0.683	0.026	7	0.374	0.015	7
138	19.300	0.038	5	0.540	0.095	6	0.385	0.074	5
141	16.863	0.012	8	0.654	0.014	8	0.438	0.012	8
142	18.711	0.025	6	1.416	0.033	5	0.881	0.021	5
143	17.640	0.012	8	0.655	0.032	8	0.448	0.008	8
144	16.535	0.007	8	0.787	0.011	9	0.492	0.014	8
145	17.264	0.077	7	0.312	0.028	7	0.320	0.030	7
146	15.917	0.059	8	0.321	0.030	8	0.347	0.055	8
147	15.945	0.016	6	0.831	0.014	6	0.523	0.013	6

TABLE 3
Mean Photometry for NGC 7006

name	V	m.e.	n	B-V	m.e.	n	V-R	m.e.	n	name	V	m.e.	n	B-V	m.e.	n	V-R	m.e.	n
1	17.323	0.013	7	1.102	0.031	5	0.698	0.025	7	111	17.018	0.010	7	1.175	0.013	7	0.627	0.005	8
5	15.756	0.005	7	1.031	0.011	7	0.557	0.007	8	112	13.972	0.010	9	1.087	0.008	10	0.585	0.004	9
6	17.989	0.014	9	0.736	0.018	9	0.461	0.013	8	115	18.970	0.023	10	1.312	0.042	9	0.701	0.030	10
7	12.810	0.009	8	0.474	0.012	9	0.293	0.005	8	117	18.602	0.015	9	0.626	0.029	10	0.387	0.026	10
8	19.483	0.041	7	0.789	0.043	5	0.464	0.014	6	119	18.844	0.015	6	0.254	0.048	6	0.068	0.022	6
9	19.024	0.040	4	0.497	0.052	4	0.241	0.033	4	122	18.984	0.054	3	0.553	0.095	3	0.349	0.073	3
12	18.096	0.007	10	1.042	0.013	9	0.568	0.011	10	124	18.111	0.033	9	0.803	0.034	9	0.457	0.034	9
14	18.920	0.021	8	0.599	0.040	8	0.427	0.040	9	127	17.653	0.011	7	1.005	0.027	5	0.589	0.013	7
15	18.291	0.013	10	0.808	0.014	10	0.472	0.008	9	132	16.919	0.010	9	1.091	0.012	9	0.574	0.008	10
16	13.598	0.005	6	0.591	0.013	7	0.346	0.004	7	134	15.217	0.005	4	0.955	0.006	4	0.536	0.003	4
17	16.485	0.005	9	0.822	0.011	10	0.438	0.007	10	148	18.809	0.017	8	0.603	0.056	9	0.400	0.029	8
19	15.514	0.011	9	0.659	0.009	10	0.360	0.006	9	150	19.101	0.033	5	0.128	0.064	4	-0.034	0.098	5
24	19.020	0.023	8	0.491	0.027	8	0.315	0.027	9	153	18.753	0.019	10	0.561	0.017	9	0.332	0.016	10
25	16.472	0.005	9	1.305	0.005	9	0.775	0.003	9	157	18.324	0.033	5	0.753	0.018	4	0.420	0.006	4
27	18.323	0.006	8	0.766	0.017	8	0.428	0.012	9	162	18.153	0.022	7	0.787	0.031	7	0.417	0.019	7
29	19.074	0.036	6	0.724	0.023	6	0.354	0.013	6	163	18.712	0.013	8	0.201	0.028	7	0.188	0.017	7
30	18.838	0.013	4	0.690	0.022	4	0.445	0.023	4	164	18.917	0.036	9	1.080	0.055	8	0.507	0.040	9
31	16.777	0.005	9	0.940	0.008	10	0.541	0.006	10	165	18.690	0.021	7	0.229	0.030	5	0.131	0.021	6
33	19.813	0.025	3	0.897	0.164	3	0.314	0.050	3	166	17.464	0.010	9	1.019	0.015	10	0.560	0.009	10
34	17.924	0.009	9	0.964	0.015	9	0.545	0.012	9	167	19.926	0.046	3	0.720	0.018	3	0.344	0.048	3
35	18.861	0.014	8	0.616	0.053	8	0.350	0.023	8	168	18.820	0.014	9	0.892	0.031	9	0.518	0.015	9
36	18.808	0.014	7	0.618	0.025	6	0.380	0.010	6	169	18.138	0.008	7	0.966	0.027	7	0.544	0.009	7
37	18.866	0.022	9	0.620	0.039	9	0.365	0.040	9	170	16.257	0.004	9	1.390	0.011	10	0.730	0.003	9
39	16.139	0.010	8	0.818	0.010	8	0.444	0.007	8	173	19.735	0.044	4	0.727	0.061	4	0.536	0.095	5
40	18.883	0.010	7	0.537	0.053	8	0.327	0.035	8	175	18.800	0.016	10	0.519	0.011	9	0.361	0.030	10
41	18.950	0.022	8	0.617	0.031	9	0.423	0.017	8	176	18.985	0.022	8	0.610	0.033	8	0.392	0.025	9
42	18.617	0.015	9	1.007	0.036	9	0.631	0.022	9	177	18.444	0.014	10	0.894	0.026	9	0.472	0.018	9
43	18.455	0.010	9	0.866	0.023	10	0.505	0.022	10	179	17.945	0.012	8	0.802	0.020	8	0.493	0.014	9
44	18.873	0.022	8	0.454	0.030	8	0.296	0.021	8	182	17.865	0.012	10	0.870	0.026	10	0.509	0.010	9
46	19.298	0.023	6	0.716	0.044	6	0.351	0.058	7	183	16.270	0.004	9	1.180	0.008	9	0.638	0.003	9
48	19.676	0.021	4	0.999	0.036	3	0.520	0.033	5	184	17.664	0.015	8	0.901	0.016	8	0.529	0.012	8
49	19.117	0.021	5	0.052	0.034	5	0.016	0.041	5	185	19.882	0.022	3	0.961	0.134	3	0.590	0.039	3
50	19.068	0.020	8	0.419	0.046	9	0.252	0.030	8	186	19.448	0.038	6	0.816	0.059	6	0.554	0.045	6
51	18.945	0.021	8	0.910	0.038	8	0.497	0.034	8	187	18.738	0.027	9	0.918	0.019	8	0.463	0.026	9
52	18.647	0.010	10	0.900	0.030	9	0.502	0.015	9	188	16.637	0.006	8	0.959	0.018	8	0.523	0.009	8
53	19.562	0.007	4	1.016	0.075	4	0.406	0.059	4	189	18.884	0.026	6	0.165	0.033	6	0.086	0.069	6
55	19.609	0.041	5	1.054	0.088	3	0.800	0.057	5	191	18.746	0.015	8	0.721	0.032	9	0.345	0.023	8
56	17.544	0.006	8	0.979	0.010	8	0.546	0.006	8	192	19.548	0.037	6	1.202	0.072	5	0.390	0.055	6
57	18.943	0.019	10	0.573	0.035	9	0.356	0.035	10	193	19.370	0.020	6	1.092	0.046	5	0.591	0.038	7
60	16.587	0.005	9	1.254	0.015	9	0.681	0.004	9	194	19.328	0.048	5	0.836	0.077	5	0.405	0.085	6
61	18.812	0.016	8	0.750	0.028	8	0.373	0.027	9	196	16.679	0.007	8	0.943	0.006	8	0.526	0.006	8
65	17.585	0.013	9	0.941	0.013	9	0.537	0.010	9	198	19.420	0.027	6	1.131	0.040	3	1.003	0.018	6
66	17.225	0.007	7	0.836	0.008	7	0.436	0.008	7	199	16.721	0.005	4	0.655	0.023	4	0.402	0.015	4
68	17.601	0.011	8	1.042	0.014	8	0.578	0.013	8	200	18.848	0.024	9	0.677	0.042	8	0.372	0.038	9
69	18.631	0.014	9	0.673	0.030	10	0.419	0.026	10	202	18.843	0.009	9	0.636	0.030	8	0.377	0.014	9
75	18.631	0.050	9	0.566	0.029	8	0.324	0.029	8	203	19.145	0.024	3	0.925	0.021	3	0.587	0.037	3
79	19.021	0.026	9	0.480	0.054	9	0.281	0.037	10	205	19.420	0.026	4	0.733	0.040	4	0.486	0.038	4
86	16.815	0.005	9	1.211	0.012	10	0.663	0.007	9	206	19.687	0.063	4	0.684	0.068	3	0.493	0.020	4
89	13.854	0.012	9	0.819	0.005	9	0.452	0.007	9	207	17.944	0.013	4	0.893	0.027	4	0.536	0.021	4
93	19.227	0.015	4	0.139	0.062	4	-0.179	0.042	4	208	19.697	0.032	3	0.944	0.084	3	0.382	0.056	3
97	18.405	0.020	8	0.656	0.048	7	0.400	0.020	9	209	14.907	0.008	3	0.992	0.006	3	0.541	0.005	3
102	18.922	0.016	8	0.429	0.025	8	0.189	0.028	9	212	18.846	0.009	3	0.651	0.021	3	0.274	0.026	3
109	19.122	0.021	7	0.860	0.159	6	0.391	0.047	7	213	18.362	0.046	3	0.874	0.010	3	0.346	0.034	3
110	17.479	0.013	10	1.033	0.017	9	0.617	0.014	10	214	17.970	0.011	3	0.889	0.045	3	0.537	0.016	3

1987, 1990) would be desirable, especially for faint images, but automated versions of such codes were not available at the inception of this project. The PSF fitting techniques are typically used in order to decrease the effects of crowding due to nearby stellar images. In our case, the problems associated with crowded field photometry encountered with aperture integration are not important. Only uncrowded stellar images will be suitable for calibrating the photographic images of the POSS survey project. It should be noted that our adopted method of applying an aperture correction using a single gaussian fit to the wings of the stellar PSF is somewhat lacking when compared to a full two-dimensional fit of the PSF. As noted by King (1971), a single gaussian is a poor fit to the entire stellar profile. Systematic errors in our photometry may be present at faint levels ($V \geq 18$), but are probably buried well below the level of observational scatter. In any case, we have

made extensive comparisons between instrumental magnitudes derived from our adopted code and those computed with DAOPHOT. In Fig. 1 we show a typical comparison between the two codes. No systematic trends are evident down to the survey limit of $V=22$. Through comparisons with a third independent source of data, we have established that the PSF fitting approach does produce a marginally reduced scatter at faint magnitudes, but the noise produced by the aperture integration algorithm has been found to be acceptably low.

The remainder of the CAPRED package handles the matching of stellar images from the six CCD images observed for each field, derivation of the extinction and photometric transformation coefficients [Eqs. (1)–(3)], and the production of transformed magnitude tables and finding charts. The image sets for NGC 7006, NGC 7790, and NGC 4147 were always used as standards for transforma-

TABLE 4
Mean photometry for NGC 7790

name	V	m.e.	n	B - V	m.e.	n	V - R	m.e.	n	name	V	m.e.	n	B - V	m.e.	n	V - R	m.e.	n
8	16.308	0.004	8	0.661	0.010	8	0.394	0.022	8	68	17.689	0.021	19	1.114	0.031	18	0.668	0.010	18
9	17.120	0.023	18	1.004	0.022	19	0.592	0.014	19	69	17.876	0.016	17	1.032	0.033	18	0.586	0.021	18
10	17.577	0.017	18	0.928	0.025	18	0.548	0.017	18	70	18.107	0.022	11	1.160	0.063	7	0.688	0.030	11
11	16.993	0.018	17	0.864	0.016	16	0.539	0.020	16	71	18.129	0.017	11	1.331	0.078	9	0.654	0.054	11
12	18.070	0.023	16	0.964	0.042	15	0.615	0.028	16	72	11.218	0.005	21	0.511	0.004	21	0.335	0.001	20
14	17.968	0.025	16	1.601	0.033	9	0.918	0.034	16	73	16.161	0.007	20	1.144	0.010	19	0.631	0.007	20
15	18.484	0.028	7	1.349	0.089	4	0.671	0.036	7	74	17.407	0.024	21	0.960	0.030	21	0.596	0.016	20
16	15.941	0.006	12	0.591	0.012	13	0.338	0.009	12	75	17.898	0.020	17	0.944	0.036	16	0.601	0.026	17
17	15.732	0.006	13	0.517	0.011	10	0.289	0.005	14	76	18.194	0.051	9	0.745	0.061	9	0.414	0.047	8
18	18.332	0.029	13	1.214	0.074	8	0.630	0.049	13	77	16.012	0.005	20	0.726	0.009	21	0.445	0.008	21
20	15.696	0.003	19	0.548	0.005	19	0.316	0.007	20	78	18.025	0.023	18	0.927	0.053	18	0.572	0.037	18
21	16.029	0.007	19	0.551	0.008	19	0.289	0.009	20	79	17.927	0.021	19	1.260	0.053	18	0.712	0.029	19
22	15.766	0.007	20	1.449	0.012	20	0.859	0.008	20	80	15.616	0.001	20	0.511	0.006	20	0.297	0.006	20
23	14.997	0.006	15	1.596	0.011	14	0.914	0.005	14	81	17.371	0.018	21	1.668	0.026	19	0.971	0.018	20
24	16.622	0.012	9	0.666	0.009	9	0.377	0.019	10	82	13.152	0.006	21	0.189	0.001	21	0.271	0.005	20
25	15.791	0.006	16	0.972	0.013	16	0.543	0.008	17	83	16.078	0.005	19	0.792	0.007	18	0.467	0.009	19
26	16.715	0.013	11	0.805	0.011	11	0.448	0.026	11	84	18.485	0.066	9	1.182	0.078	7	0.831	0.051	8
27	17.575	0.025	20	0.923	0.022	18	0.523	0.027	20	85	16.685	0.018	18	0.967	0.020	19	0.574	0.019	19
28	16.919	0.014	13	0.764	0.019	12	0.434	0.017	13	86	16.724	0.010	11	0.995	0.006	11	0.617	0.012	12
29	13.305	0.006	21	0.391	0.004	21	0.248	0.005	20	87	17.860	0.014	19	0.861	0.031	19	0.557	0.024	20
30	13.474	0.006	21	0.406	0.004	21	0.251	0.005	20	88	15.795	0.004	20	0.993	0.004	20	0.566	0.004	21
31	13.597	0.003	16	0.445	0.005	16	0.287	0.004	16	89	18.709	0.041	8	0.975	0.082	4	0.713	0.029	7
32	15.402	0.007	8	0.594	0.010	6	0.353	0.006	9	90	17.654	0.014	16	0.895	0.021	16	0.566	0.020	16
34	17.724	0.018	18	0.898	0.015	18	0.555	0.023	19	91	18.229	0.031	15	1.136	0.059	15	0.619	0.038	15
35	18.391	0.055	9	0.985	0.063	7	0.680	0.063	8	92	18.518	0.043	9	1.000	0.083	9	0.597	0.069	9
36	14.526	0.004	20	0.485	0.004	20	0.299	0.005	20	93	18.066	0.016	14	1.327	0.042	12	0.822	0.024	15
37	14.724	0.004	21	0.467	0.004	21	0.282	0.004	21	94	16.129	0.008	20	0.694	0.007	19	0.422	0.006	19
38	16.132	0.007	21	0.647	0.010	20	0.374	0.010	21	95	15.829	0.006	18	0.583	0.007	17	0.341	0.007	18
39	17.622	0.014	20	1.169	0.025	19	0.662	0.019	21	96	15.787	0.009	20	0.708	0.004	19	0.416	0.006	19
40	17.740	0.014	21	1.217	0.031	18	0.726	0.011	20	97	13.189	0.005	19	1.491	0.005	19	0.819	0.004	19
41	17.709	0.015	21	0.892	0.020	19	0.526	0.025	21	98	14.126	0.003	20	0.800	0.003	20	0.474	0.003	19
42	17.589	0.025	20	1.129	0.033	20	0.669	0.020	19	99	16.761	0.018	19	0.791	0.017	19	0.435	0.009	20
43	18.317	0.027	15	1.016	0.037	14	0.603	0.036	15	100	17.820	0.021	20	1.143	0.034	20	0.692	0.027	20
44	18.388	0.049	9	1.147	0.072	8	0.691	0.043	8	101	18.078	0.021	17	1.005	0.037	17	0.634	0.033	18
45	15.778	0.007	13	0.561	0.010	13	0.312	0.007	12	103	16.761	0.010	20	0.779	0.012	20	0.436	0.008	20
46	17.901	0.022	16	1.046	0.017	15	0.644	0.022	16	104	15.227	0.006	18	0.538	0.006	17	0.318	0.007	18
47	18.377	0.031	11	1.229	0.040	6	0.827	0.047	11	105	15.704	0.005	19	1.896	0.015	20	1.092	0.007	20
48	15.261	0.004	17	0.857	0.008	17	0.519	0.001	17	106	17.433	0.019	20	1.139	0.021	21	0.679	0.017	20
49	16.573	0.010	17	1.687	0.021	17	1.008	0.013	17	107	15.362	0.005	19	1.939	0.013	19	1.116	0.007	19
50	17.896	0.020	18	1.714	0.060	12	1.005	0.019	18	108	17.175	0.016	20	1.147	0.024	20	0.654	0.016	19
51	14.130	0.004	14	0.419	0.004	13	0.251	0.004	13	109	17.433	0.016	10	0.997	0.024	11	0.599	0.029	11
52	17.561	0.018	17	1.661	0.034	15	1.026	0.018	18	110	16.683	0.019	10	1.145	0.020	10	0.717	0.016	10
53	16.323	0.012	20	0.626	0.010	20	0.343	0.009	21	111	18.598	0.029	3	1.055	0.040	3	0.668	0.032	3
54	16.559	0.010	20	1.003	0.023	21	0.612	0.011	21	112	16.528	0.006	19	1.119	0.014	19	0.668	0.009	20
55	17.919	0.018	18	0.985	0.033	18	0.563	0.026	18	113	14.868	0.004	18	0.484	0.005	18	0.316	0.005	17
56	18.301	0.027	14	0.874	0.042	14	0.579	0.038	14	114	17.159	0.015	18	1.037	0.020	19	0.617	0.016	19
57	18.788	0.029	6	1.177	0.093	5	0.691	0.033	6	115	17.616	0.019	19	1.142	0.024	19	0.668	0.025	19
58	15.291	0.003	19	0.610	0.005	19	0.350	0.005	20	116	17.833	0.016	20	1.593	0.039	12	0.988	0.024	20
59	15.976	0.006	20	0.559	0.005	20	0.315	0.007	20	117	18.177	0.015	3	1.034	0.052	3	0.646	0.060	3
60	16.804	0.014	21	1.177	0.021	21	0.640	0.010	20	119	18.285	0.025	10	0.943	0.061	10	0.612	0.022	10
61	18.636	0.021	6	1.030	0.071	5	0.493	0.054	6	121	17.994	0.038	8	1.005	0.091	8	0.580	0.035	7
62	15.123	0.001	17	1.667	0.005	17	0.974	0.003	18	122	18.509	0.022	4	1.674	0.190	3	1.284	0.030	4
63	18.554	0.043	9	1.179	0.096	10	0.546	0.070	10	123	15.671	0.007	5	1.447	0.015	5	0.876	0.008	5
64	18.733	0.036	12	1.293	0.109	6	0.594	0.045	11	124	18.451	0.041	6	1.092	0.055	6	0.634	0.042	6
65	16.045	0.005	16	0.709	0.005	16	0.409	0.008	15	125	17.307	0.020	11	1.093	0.039	11	0.584	0.016	11
66	15.939	0.006	16	0.572	0.009	16	0.328	0.010	16	126	17.629	0.011	9	0.954	0.016	9	0.564	0.021	9
67	17.013	0.012	16	0.859	0.015	16	0.522	0.013	17	127	17.830	0.025	6	1.092	0.056	6	0.650	0.021	7

tion to the Cousins system, but in the last stage of each reduction all stellar images on these frames were transformed from the instrumental to the standard system in the same manner as the program fields. The transformed magnitude files for these standard clusters from the nights listed in Table 1 were used in the statistical analysis discussed in the next section.

3. DERIVATION OF THE MEAN MAGNITUDES

All of the magnitude files for each cluster set were matched to a master coordinate system via a linear coordinate transformation. A simple database manager was then used to evaluate the BVR magnitudes for each star. For each set of magnitudes we have computed the mean,

median, and standard deviation about the mean. An iterative rejection process was used to exclude discrepant data points. In each iteration the largest residual relative to the median was eliminated from the sample and the mean and standard deviation recomputed. If the standard deviation was decreased by at least 20%, then the point was permanently eliminated from the sample and the rejection process continued. A maximum of three rejection iterations was performed for each star. Rejection about the median proved to be very robust and 11 stars were found to give occasionally poor magnitudes. In each case the bad data points were found to be the result of field crowding effects on images taken under very poor seeing conditions. Because it was our intent to form a mean list of uncrowded

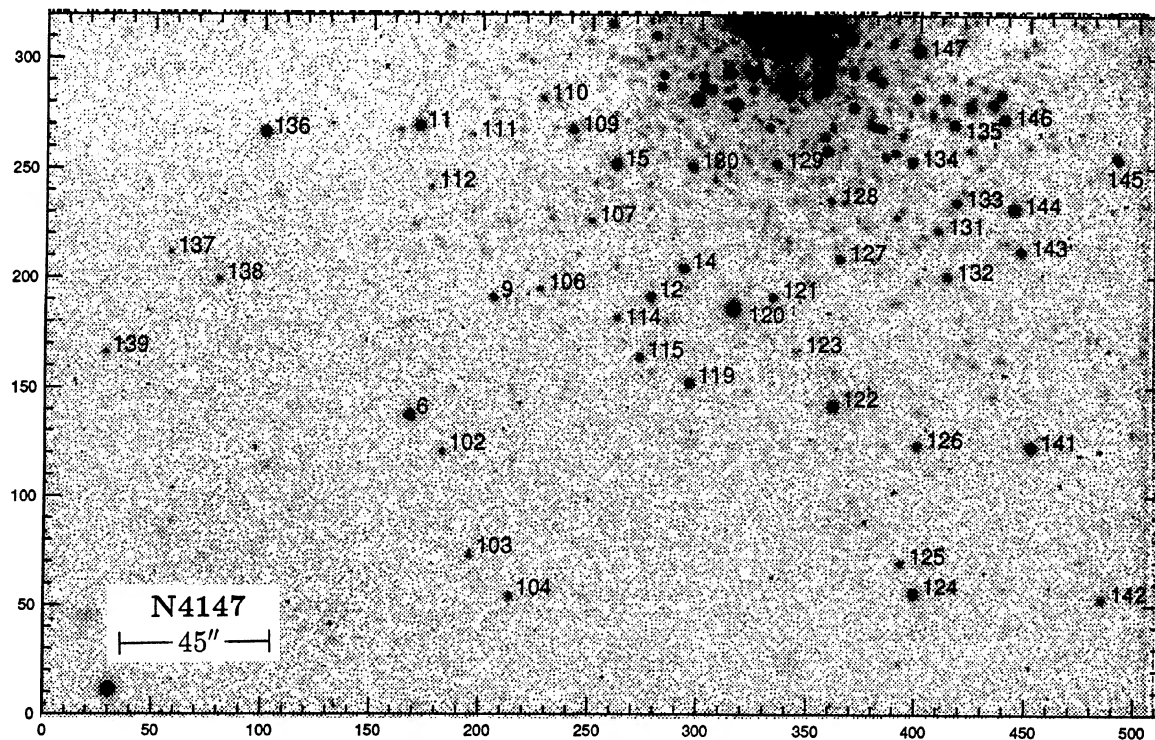


FIG. 3—Finding chart for the new NGC 4147 standard field. Star names given in Table 2 are plotted to the right of each star in the sequence. North is at the top and east is to the left. Coordinates on the axes are plotted in pixel units (1 pixel=0.654 arcsec).

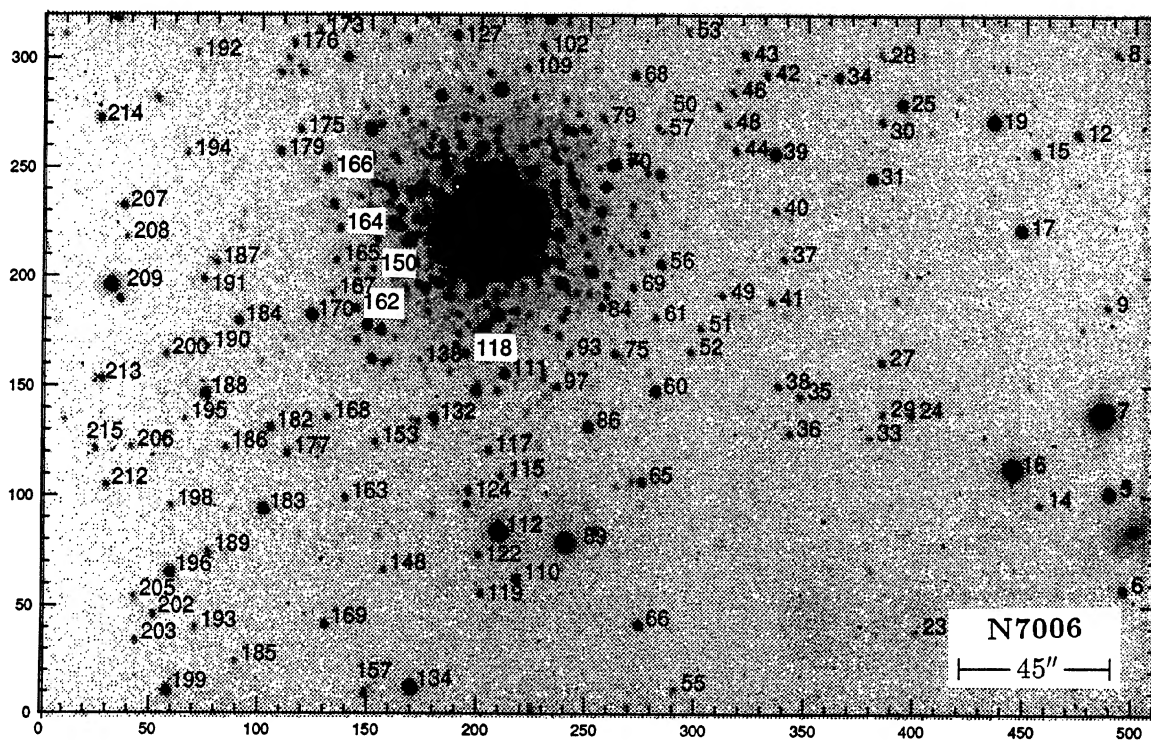


FIG. 4—Finding chart for the new NGC 7006 standard field. Star names given in Table 3 are plotted to the right of each star in the sequence. North is at the top and east is to the left. Coordinates on the axes are plotted in pixel units (1 pixel=0.654 arcsec).

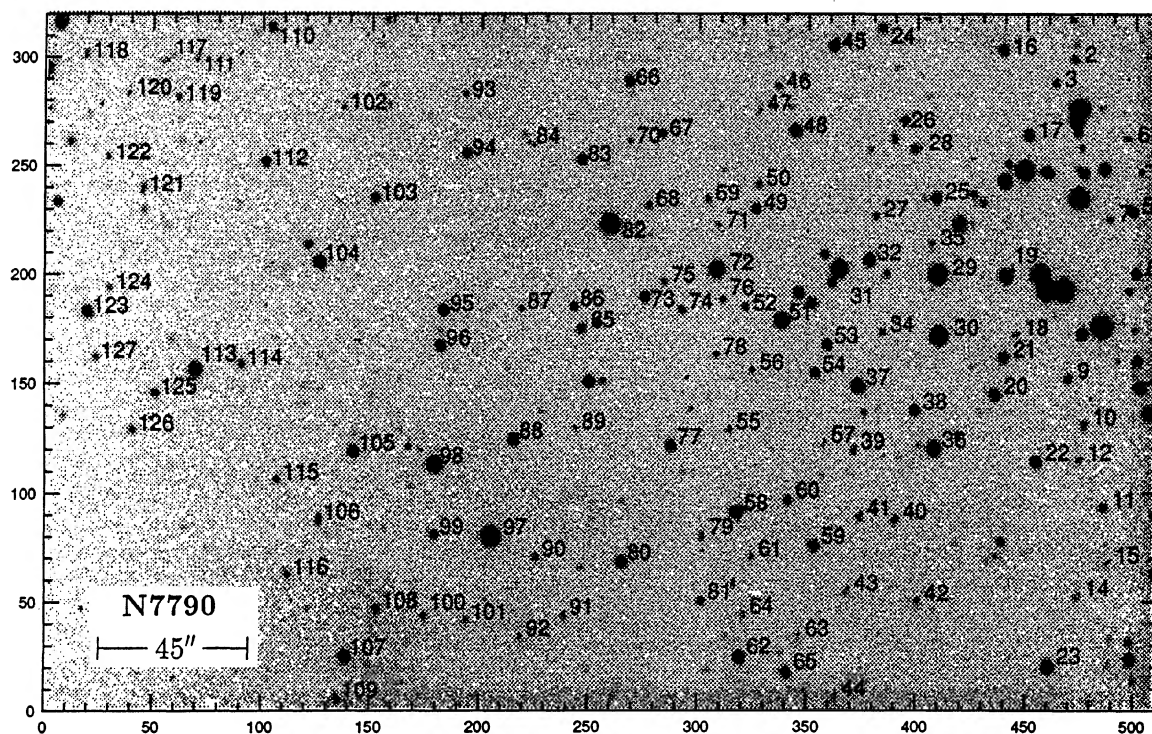


FIG. 5—Finding chart for the new NGC 7790 standard field. Star names given in Table 4 are plotted to the right of each star in the sequence. North is at the top and east is to the left. Coordinates on the axes are plotted in pixel units (1 pixel=0.654 arcsec).

stellar images, these objects were eliminated from the final magnitude tabulations. In Fig. 2 we show a plot of magnitude versus Julian Date for a typical set of magnitude measurements. Circled points indicate measurements eliminated in the rejection process. These plots were used to confirm that the rejected points were indeed discrepant observations and to search for possible long-term variable stars. It should be noted that each set of V , $B-V$, and $V-R$ is treated independently at the point of deriving mean values. This procedure will occasionally permit a point to be accepted in one or two passbands, but be rejected in another. An improved analysis might require that a point rejected for a star in one bandpass on a given night should nullify the use of the other bandpass measurements for that star on that night.

In Tables 2-4 we tabulate the final mean magnitudes and colors for the stars in each sequence, the mean errors of the means, and the numbers of observations used to compute mean values. For the sake of compactness we have not tabulated the relative X, Y positions of each star in the photometry tables published here. However, the electronic versions of these tables, which do include the X, Y coordinates, are available upon request (sco@aps1.spa.umn.edu). Finding charts for the new sequences are shown in Figs. 3-5. A star identification number is printed to the right of each star. In Figs. 6-8 we plot the estimated mean error in V , $B-V$, and $V-R$ as a function of V magnitude to demonstrate the greatly decreased scatter in the final mean photometry.

In addition to establishing a set of magnitudes with ob-

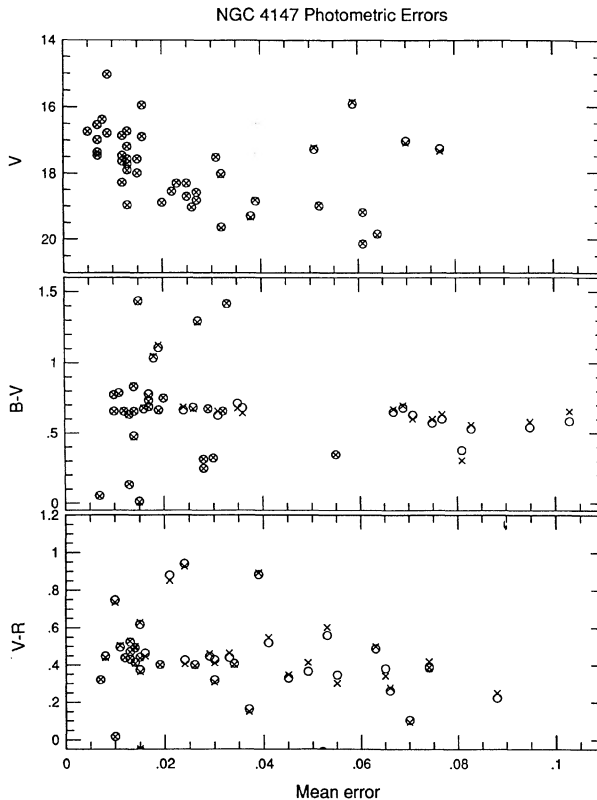


FIG. 6—Mean (open circle) and median (crosses) V , $B-V$, and $V-R$ values as a function of estimated mean error for the NGC 4147 sample. This standard sequence was computed from nine nights of observations.

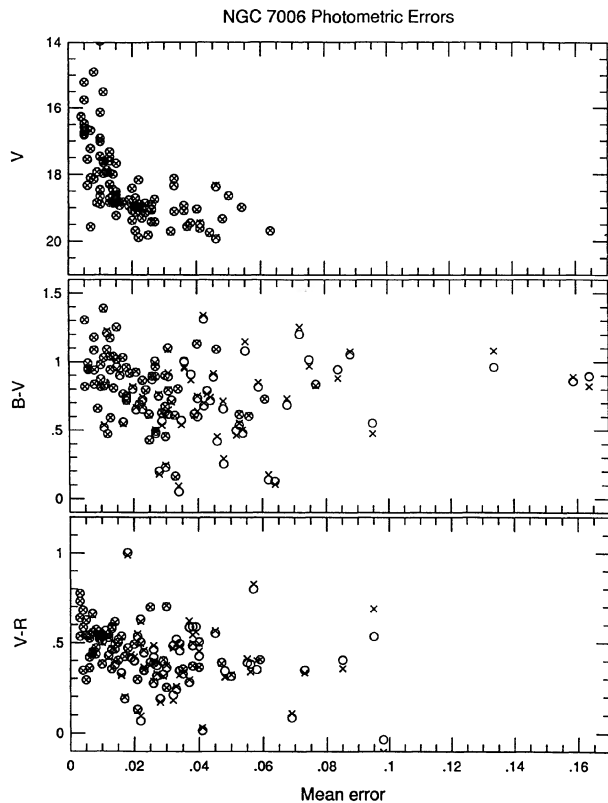


FIG. 7—Mean (open circle) and median (crosses) V , $B-V$, and $V-R$ values as a function of estimated mean error for the NGC 7006 sample. This standard sequence was computed from ten nights of observations.

jectively determined errors, we have increased the usable color range in the standard fields by pushing the sequences to fainter limits. It should be stressed that the present analysis serves only to decrease and quantify the amount of accidental scatter in the photometry. Since our color transformation coefficients and zero-point terms are tied to the C85 photometry, any systematic errors associated with that photometry (Stetson and Harris 1988) will remain in our data. Full assessment of the external errors of this photometry will require independently calibrated all-sky photometry.

We wish to thank L. Davis for the use of her NGC 7790 photometry prior to publication. We also wish to thank R. L. Pennington, W. A. Zumach, and members of the staff of the Capilla Peak Observatory for their assistance in obtaining the CCD observations. This work is supported by the

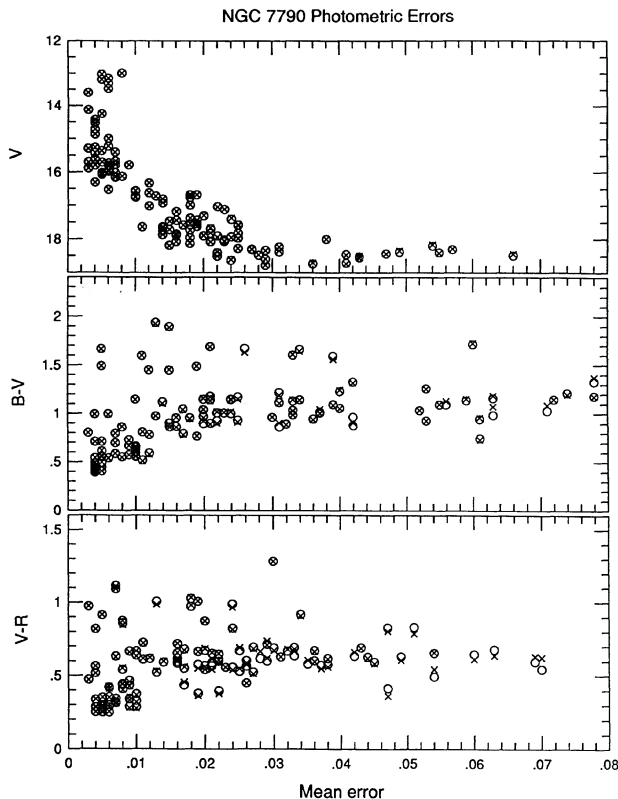


FIG. 8—Mean (open circle) and median (crosses) V , $B-V$, and $V-R$ values as a function of estimated mean error for the NGC 7790 sample. This standard sequence was computed from 21 nights of observations.

National Science Foundation under Grant No. AST88-15867.

REFERENCES

- Beckert, D. C., and Newberry, M. V. 1989, *PASP*, 101, 849
 Christian, C. A., Adams, M., Barnes, J. V., Butcher, H., Hayes, D. S., Mould, J. R., and Siegel, M. 1985, *PASP*, 97, 363
 King, I. R. 1971, *PASP*, 83, 199
 Humphreys, R. M., Landau, R., Ghigo, F., Zumach, W., and Labonte, A. E., 1991, *AJ*, 102, 395
 Landolt, A. U. 1973, *AJ*, 78, 959
 Pennington, R. L., Humphreys, R. M., Zumach, W. A., and Odewahn, S. C. 1991, in *Digitized Optical Sky Surveys*, ed. H. T. MacGillivray, to be published
 Stetson, P. B. 1990, *PASP*, 102, 932
 Stetson, P. B., and Harris, W. E. 1988, *AJ*, 96, 909
 Stetson, P. B. 1987, *PASP*, 99, 191